



ABLATION AND CHEMICAL ALTERATION OF COSMIC DUST PARTICLES DURING ENTRY INTO THE EARTH'S ATMOSPHERE

N. G. RUDRASWAMI¹, M. SHYAM PRASAD¹, S. DEY^{1,2}, J. M. C. PLANE³, W. FENG^{3,4}, J. D. CARRILLO-SÁNCHEZ³, AND D. FERNANDES¹

¹ National Institute of Oceanography (Council of Scientific and Industrial Research), Dona Paula, Goa 403004, India; rudra@nio.org

² Indian Institute of Technology, Roorkee, Uttarakhand 247667, India

³ School of Chemistry, University of Leeds, Leeds LS2 9JT, UK

⁴ NCAS, School of Earth and Environment, University of Leeds, Leeds, LS2 9JT, UK

Received 2016 September 11; revised 2016 October 28; accepted 2016 November 5; published 2016 December 2

ABSTRACT

Most dust-sized cosmic particles undergo ablation and chemical alteration during atmospheric entry, which alters their original properties. A comprehensive understanding of this process is essential in order to decipher their pre-entry characteristics. The purpose of the study is to illustrate the process of vaporization of different elements for various entry parameters. The numerical results for particles of various sizes and various zenith angles are treated in order to understand the changes in chemical composition that the particles undergo as they enter the atmosphere. Particles with large sizes ($>$ few hundred μm) and high entry velocities ($>16 \text{ km s}^{-1}$) experience less time at peak temperatures compared to those that have lower velocities. Model calculations suggest that particles can survive with an entry velocity of 11 km s^{-1} and zenith angles (ZA) of 30° – 90° , which accounts for $\sim 66\%$ of the region where particles retain their identities. Our results suggest that the changes in chemical composition of MgO, SiO₂, and FeO are not significant for an entry velocity of 11 km s^{-1} and sizes $<300 \mu\text{m}$, but the changes in these compositions become significant beyond this size, where FeO is lost to a major extent. However, at 16 km s^{-1} the changes in MgO, SiO₂, and FeO are very intense, which is also reflected in Mg/Si, Fe/Si, Ca/Si, and Al/Si ratios, even for particles with a size of $100 \mu\text{m}$. Beyond $400 \mu\text{m}$ particle sizes at 16 km s^{-1} , most of the major elements are vaporized, leaving the refractory elements, Al and Ca, suspended in the troposphere.

Key words: atmospheric effects – Earth – interplanetary medium – minor planets, asteroids: general – Sun: general

1. INTRODUCTION

Earth is continuously bombarded by high-speed particles from both incoming asteroidal and cometary material. Although efforts have been made to learn the exact contributions from each of these sources, such efforts are nevertheless hampered by large levels of uncertainties (e.g., Plane 2012). Micrometeorites are the largest contributors of extra-terrestrial material; this material is recovered from the Earth's surface using different collection techniques that target the stratosphere, Antarctica, and deep-sea sediments (Love & Brownlee 1993; Taylor et al. 1998; Peucker-Ehrenbrink & Ravizza 2000; Plane 2012; Prasad et al. 2013). The micrometeorites found on the Earth's surface have distinct chemical compositions that show similarities and differences with respect to the precursors they originate from; however, in general, a large number of micrometeorites are related to carbonaceous chondrites (e.g., Kurat et al. 1994; Brownlee et al. 1997; Taylor et al. 2000, 2012; Yada et al. 2005; Rudraswami et al. 2011, 2012, 2014, 2015a, 2015b, 2016a). The deviations in the chemical compositions from the precursors are caused by modification that occurs during melting and vaporization that take place as these particles enter into the Earth's atmosphere. These modifications are dominated by a loss of elements based on their relative volatilities, and other physical processes that are parameterized by key variables such as size, density, entry velocity, and angle of entry, in addition to others (Love & Brownlee 1991; Rudraswami et al. 2015a, 2016a). The origin of micrometeorites is currently debated, whether the micrometeorites are asteroidal or cometary, and to what extent the origin

contributes to the micrometeorites' flux is also debated (Dermott et al. 1994; Brownlee 2001; Nesvorný et al. 2010, 2011). The other potential source that has been suggested is fragmentation of large objects that hit the atmosphere (Lal & Jull 2002). This has not been supported by micrometeorite chemical analyses, which are inclined toward the major contributor being carbonaceous chondrites, whereas a majority of meteorites are from ordinary chondrites (Krot et al. 2003; Taylor et al. 2007). In addition, large cosmic spherules such as glass spherules do not entirely support the concept of fragmentation (Rudraswami et al. 2012). Moreover, the air pressure at the altitude above Earth's surface, where ablation and vaporization occur, is very low, which allows meteoritic material to fragment into such small particles, even in material with small tensile strength. Nevertheless, the explanation that a combination of asteroidal and cometary materials contributes to micrometeorite flux appears to be more plausible. Cometary bodies have the best preserved solar system materials (Brownlee et al. 2006; Brownlee 2014). Getting hold of these materials that have not altered during atmospheric entry will enable us to provide an understanding of the diverse origins of these enigmatic particles in the solar nebula and provide insights into their origins. Micrometeorites' interactions with the Earth's atmosphere can be constrained properly by understanding the process of chemical composition as the micrometeorites enter at different altitudes under different conditions. Earlier model calculations largely focused on the deceleration of particles at various entry velocities, thereby estimating the ablation and temperature that the particles undergo at various sizes and entry angles (Flynn 1989a, 1989b;

Love & Brownlee 1993; Brownlee 2001; Kortenkamp et al. 2001). Our understanding of the role of elemental ablation will allow us to identify the chemical alterations experienced by the particles. In doing so, the properties of the particles before their entry can be inferred. This may possibly lead us to infer the type of precursors these particles belong to, though this will not be as easy as it seems because it will involve the association of multiple parameters that will behave similarly under different entry velocities, zenith angles, and sizes. We review our understanding of the various physical and chemical properties related to these particles; these properties are important for understanding how these particles are modified from their original identities. The change in chemical composition during entry depends on various parameters (entry velocity, mass, density, zenith angle (ZA), and chemical composition) of entering particles. The compositional variation during entry and the elemental volatility control the bulk chemical composition and hence bulk chemical composition alone is inadequate to resolve our understanding of precursors.

Numerical calculations are significant for quantifying the interactions that lead to chemical and physical modifications during atmospheric entry. Numerical calculations will also be a useful parameter for providing estimates of the flux, which has so far been assessed with multiple values (Taylor et al. 1998; Yada et al. 2004; Plane 2012; Prasad et al. 2013). We use the Chemical Ablation Model (CABMOD; Vondrak et al. 2008) to derive the ablation rate profiles of the most abundant elements as a function of the altitude for each meteoroid with a given mass, velocity, and entry angle after it enters the atmosphere. The present study focuses on understanding the physical modification associated with chemical alteration that incoming particles undergo during entry; this modification provides us with the probability of associating a particle with its predecessor. Comparison of elemental properties of micrometeorites of different sizes, entry velocities, and ZAs has revealed a number of interesting aspects of particles undergoing atmospheric entry that will be discussed in this study.

2. MODEL DETAILS

The CABMOD model includes the standard treatment of meteor physics: a balance of frictional heating by radiative losses and the absorption of heat energy through temperature increase, melting, phase transitions, and vaporization. (Vondrak et al. 2008; Plane 2012). The model considers the non-thermal sputtering mass-loss of particles due to inelastic collisions with air molecules before melt, followed by ionization of ablated particles, diffusion-controlled ablation of alkali metals, and Langmuir evaporation of metal atoms and oxides from molten bulk using the MAGMA chemical equilibrium code (Schaefer & Fegley 2005). The classical theory of interaction with the atmosphere treats a particle as a homogeneous sphere where heat transfer is isothermal (Vondrak et al. 2008). The emissivity considered in this study is set to 1. The emission efficiency declines when the particle size is analogous or less than the radiation wavelength (Bohren & Huffman 1983, p. 130). Earlier, Vondrak et al. (2008) took an estimate that took into account the atmospheric curvature for input particles with a high zenith angle and established that this effect is not significant. The gravity is included in Equation (1) of Vondrak et al. (2008) and its effect is seen to be insignificant in the range of velocities considered here for particle entry.

CABMOD integrates in terms of height, so it is capable of estimating the elemental deposition of different metals using MAGMA. Additional comprehensive processes related to the chemical ablation of particles for various entry parameters is given in Vondrak et al. (2008). The particle initial composition is preferred to be a CI chondritic composition that is mainly composed of olivine. The behavior of the olivine phases diagram (Figure 4(a) of Vondrak et al. 2008) suggests that the Fe/Mg ratio 0.8 starts to melt at 1730 K and becomes completely melted at 1800 K, which is considered to be the melting point of the particle. The CABMOD model includes a sigmoid temperature curve that is an empirical function that describes the depletion of the elements in a more realistic way. It should be noted that the term ablation covers both sputtering and vaporization from the molten bulk. During the ablation process, the primary composition changes to secondary composition, leading a loss of the original properties. To achieve a good computational accuracy, the integration is sampled with a vertical height resolution of 100 m. The ablation or temperature change is insignificant within vertical resolutions smaller than 100 m for any size particle, except for large entry velocities ($>16 \text{ km s}^{-1}$), where the change starts to become relevant. Our goal is to provide an overall demonstration of the particle response during atmospheric entry. The general approach of simulations during the last few decades has primarily relied on understanding the changes to the entry parameters, and thus their ramifications for the physical properties of particles, such as size and the percentage of ablation. In our study we have made an effort to identify the variation in the elemental composition associated with ablation for various entry phenomena. We have restricted the entry velocity to 16 km s^{-1} because increasing entry velocity beyond this point and working with particle sizes of $100\text{--}700 \mu\text{m}$ results in an ablation of $>90\%$, which is futile. Particles that enter the Earth's atmosphere with greater velocities will undergo large ablation due to frictional heating from striking air molecules and will lose their identities as particles. The main stream of particles that hits the upper atmosphere at $\leq 16 \text{ km s}^{-1}$ should survive the atmospheric entry, and should continue being micrometeorites (Nesvorný et al. 2011; Carrillo-Sánchez et al. 2015). Flynn (1989a, 1989b) used densities of $\sim 1 \text{ g cm}^{-3}$, which are from fluffy materials whose main sources are cometary bodies. However, further detailed micrometeorite modeling by Love & Brownlee (1991) that used various entry velocities and ZAs considered a particle density of $\sim 3 \text{ g cm}^{-3}$. The measured density of stratospheric interplanetary dust particles is dominated by particles that are $\sim 2 \text{ g cm}^{-3}$, which is consistent with those found in CI-chondrites (Love et al. 1994). The present study considers the chemical compositions and properties of entering particles that are similar to primitive CI chondritic compositions with a density of $\sim 2 \text{ g cm}^{-3}$ (Mason 1971; Sears & Dodd 1988, pp. 3–31; Lodders & Fegley 1998). The major elemental composition of micrometeorites conforms to a CI composition, as suggested by various studies (e.g., Brownlee et al. 1997; Taylor et al. 2000; Prasad et al. 2013). The majority of the dust producers in the asteroid belt are bodies that have low tensile strength and that can fragment into smaller particles during collisions; CI chondrite fits this category very well. During collisions between two asteroids, properties such as low density and high porosity can be useful for facilitating a breakdown into dust particles in the size ranges that define micrometeorites.

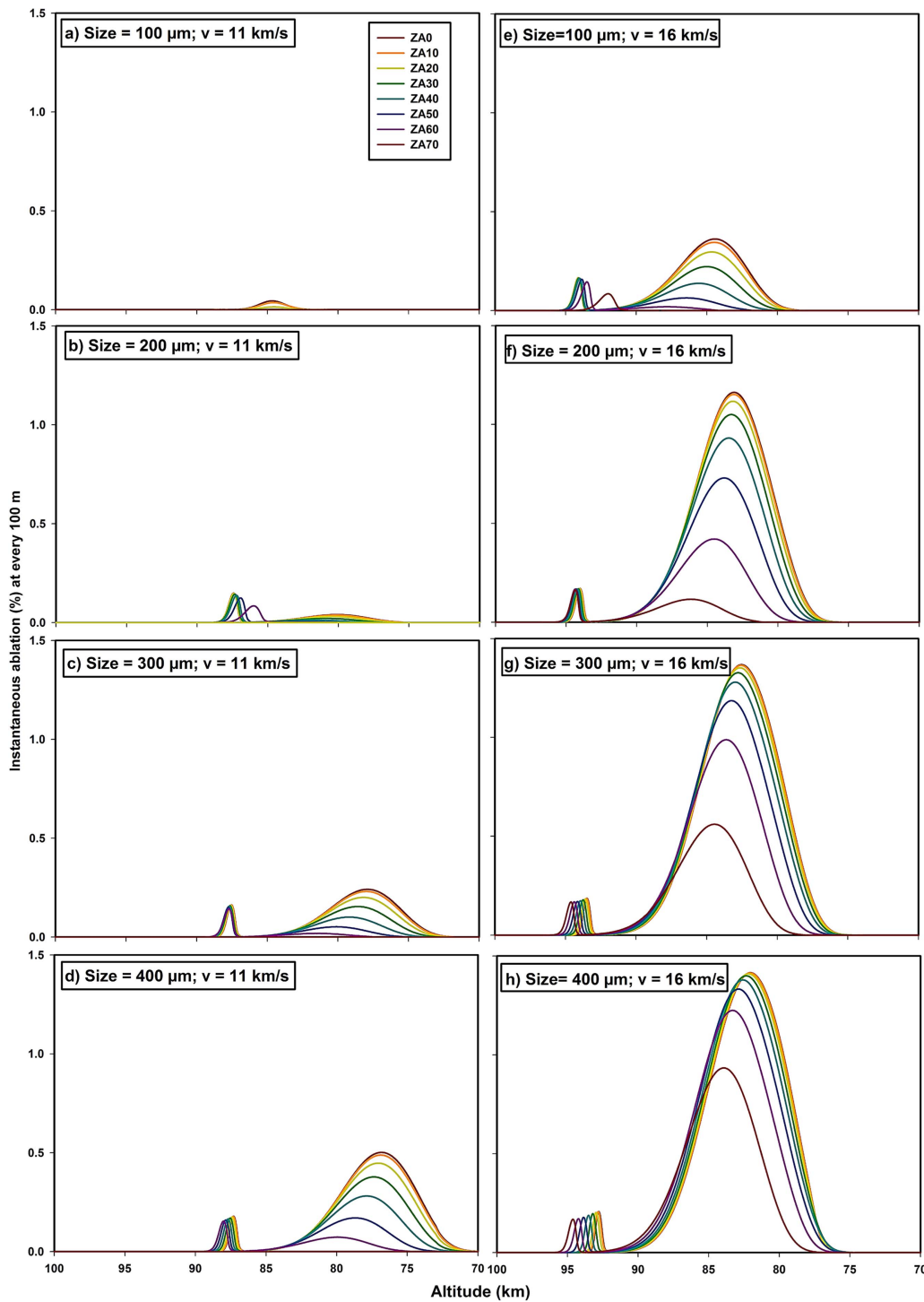


Figure 1. The representative instantaneous ablation (%) of the particle for every 100 m at various altitudes and sizes from 100 to 400 μm for various ZAs with entry velocities of 11 km s^{-1} (a–d) and 16 km s^{-1} (e–h). The first peak is for the volatile element (Na and K), followed by ablation of major elements. The ZAs 80° and 90° for both entry velocities (11 and 16 km s^{-1}) are not included, as the instantaneous ablation percent is insignificant.

Conversely, researchers have also pointed toward the contribution from cometary bodies (Nesvorný et al. 2010, 2011). The particles that are generated by asteroidal collisions have better gravitational focusing and enter an Earth resonance orbit at much lower velocities compared to cometary bodies (Flynn 1989a, 1989b; Brownlee 2001; Kortenkamp et al. 2001). The complexity of entry phenomena is reinforced by considering the combination of physical and chemical parameters and using different geometrical arrangements for the entry of particles.

3. ABLATION

Ablation is the result of vaporization that leads to a loss of mass that thereby changes the initial elemental composition as it enters the Earth’s atmosphere. The amount of ablation depends on entry parameters such as velocity, ZA, the size of the particle, and the initial composition. It is interesting to see how the particles interact with Earth’s atmosphere, generating large-scale heating due to collision with air molecules, and then

Table 1

The Data for Total Mass Ablated (%) and the Time (s) the Particles Remain at the Peak Temperature within 200 K (Provided in Brackets) for Various Sizes, ZAs, and Entry Velocities

Entry Velocity	Size (μm)	ZA = 0°	10°	20°	30°	40°	50°	60°	70°	80°	90°
11 km s ⁻¹	100	1 [1.41]	1 [1.43]	0 [1.42]	0 [1.44]	0 [1.46]	0 [1.49]	0 [1.54]	0	0	0
	200	3 [1.28]	3 [1.28]	3 [1.29]	2 [1.29]	2 [1.29]	1 [1.34]	1 [1.36]	0	0	0
	300	16 [1.24]	15 [1.24]	13 [1.24]	10 [1.24]	7 [1.25]	4 [1.26]	2 [1.26]	0	0	0
	400	33 [1.22]	32 [1.22]	29 [1.23]	25 [1.23]	18 [1.21]	11 [1.23]	5 [1.23]	0	0	0
	500	42 [1.21]	41 [1.22]	38 [1.22]	33 [1.20]	25 [1.22]	16 [1.22]	8 [1.21]	0	0	0
	600	57 [1.23]	56 [1.23]	54 [1.22]	49 [1.22]	42 [1.21]	31 [1.22]	18 [1.19]	0	0	0
	700	65 [1.23]	64 [1.24]	62 [1.22]	58 [1.23]	51 [1.21]	41 [1.20]	26 [1.18]	0	0	0
16 km s ⁻¹	100	22 [0.85]	21 [0.85]	18 [0.86]	14 [0.87]	9 [0.88]	5 [0.91]	2 [0.93]	1 [0.98]	0	0
	200	76 [0.76]	75 [0.77]	72 [0.77]	67 [0.78]	59 [0.79]	45 [0.81]	26 [0.84]	8 [1.09]	0	0
	300	93 [0.69]	93 [0.69]	92 [0.69]	89 [0.70]	85 [0.73]	77 [0.75]	62 [0.74]	35 [0.81]	0	0
	400	96 [0.68]	95 [0.69]	95 [0.69]	95 [0.69]	94 [0.68]	90 [0.70]	80 [0.70]	58 [0.77]	0	0
	500	96 [0.53]	96 [0.55]	96 [0.60]	95 [0.69]	95 [0.68]	93 [0.69]	86 [0.68]	67 [0.76]	0	0
	600	97 [0.34]	97 [0.36]	97 [0.38]	97 [0.45]	96 [0.54]	95 [0.65]	93 [0.68]	81 [0.72]	0	0
	700	97 [0.29]	97 [0.29]	97 [0.29]	97 [0.35]	97 [0.43]	96 [0.57]	95 [0.67]	87 [0.70]	0	0

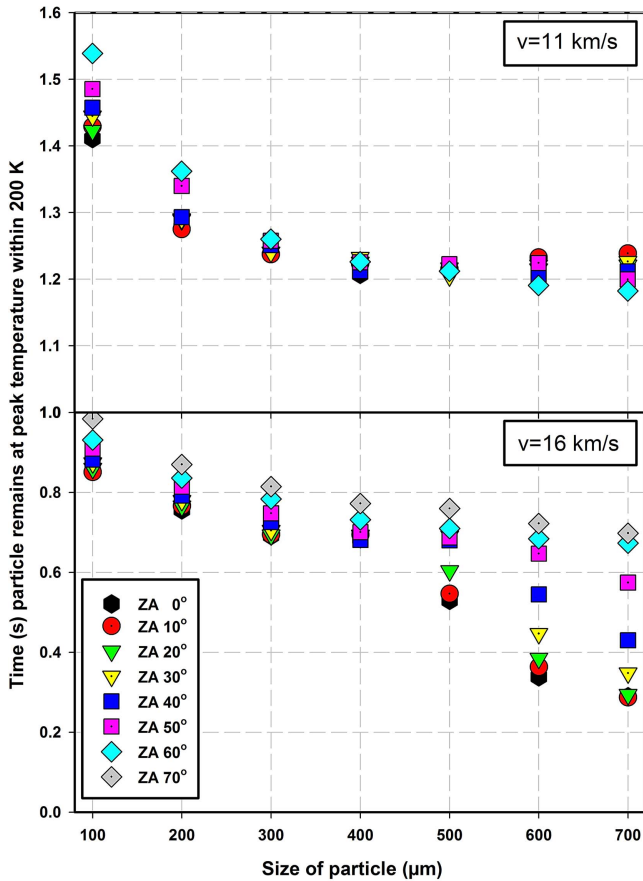


Figure 2. The time particles remain at the peak temperature within 200 K vs. the size of particles for various ZAs. The time spent at the peak temperature for 16 km s⁻¹ is much lower than that of 11 km s⁻¹. The ZAs 80° and 90° for both entry velocities (11 and 16 km s⁻¹) are excluded due to a lack of ablation. In addition, the ZA 70° for $v = 11 \text{ km s}^{-1}$ is also not included due to the non-existence of ablation.

experiencing ablation and changes in chemical composition. It is clear from Figure 1 that irrespective of entry velocity, ablation occurs at an altitude around 70–90 km. The instantaneous mass ablation represented in Figure 1 is a percentage of the mass ablated for each 100 m decrease in altitude of the particle relative to the initial mass of the particle. The ablation

or instantaneous ablation depends on the temperature that the particle reaches during its entry into the atmosphere, and terminates when the temperature and velocity drop beyond the point at which the partial or fully molten particle solidifies. Particles at high ZA travel at a low atmospheric density for longer times because their frictional heating fails to generate enough heat to raise the temperature and lead to minimum mass-loss. The time elapsed by the particle within 100 K of the peak temperature for particles with sizes of 10–20 μm is $\sim 2 \text{ s}$ (Flynn 1989a, 1989b). In the present study we consider the time elapsed by the particle at a peak temperature within 200 K, for sizes from 100 to 700 μm , as we believe the spread will have a substantial effect on modifying the chemical composition. The time that particles spend at the peak temperature varies for different sizes, ZAs, and entry velocities, as seen in Table 1. The time spent for large particles in size ranges from ~ 100 to $\sim 700 \mu\text{m}$ is from 0.3 to 1 s for various ZAs at an entry velocity of 16 km s⁻¹, while it is 1.2–1.5 s for those with an entry velocity of 11 km s⁻¹ (Figure 2). Consider two different entry velocities. (a) 16 km s⁻¹: the change in ZA does not change the time spent at the peak temperature up to 400 μm ; beyond this size ($>500 \mu\text{m}$) at lower ZA (0°–40°) the time at peak temperature shortens drastically. However, for ZAs above 50° the time change is within $\pm 0.3 \text{ s}$ for any size. (b) 11 km s⁻¹: the change in ZA does not change the time that the particle remains at the peak temperature for sizes $>300 \mu\text{m}$. There is an increase in the time at peak temperature below 300 μm , e.g., the time elapsed for $\sim 200 \mu\text{m}$ at any ZA is $\sim 1.3 \text{ s}$, while for $\sim 100 \mu\text{m}$ it is ~ 1.4 – 1.5 s (Figure 2).

The understanding gained with respect to ZA is that particles with larger sizes and smaller ZAs spend less time at the peak temperature compared to particles with large ZAs. Furthermore, those with higher entry velocities spend less time at the peak temperature than particles that enter with lower entry velocities. Although the time difference is trivial, the extent of the modification to the particles is not insignificant. A change in heating time for a fraction of a second at the peak temperature can alter the ablation significantly. It can be seen in Figure 2, at 16 km s⁻¹ for 200 μm , that the time spent at the peak temperature for ZA 0° is 0.76 s, while that for ZA 60° is 0.84 s. For 11 km s⁻¹, at ZA 0° the time spent is 1.28 s and that for ZA 60° is 1.36 s. However, at 11 km s⁻¹ and a size of 700 μm the time at the peak temperature for various ZAs is

Table 2
The Peak Temperature (K) Attained by Particles of Various Sizes and Entry Parameters

Entry Velocity	Size (μm)	ZA = 0°	10°	20°	30°	40°	50°	60°	70°	80°
11 km s ⁻¹	100	1741	1735	1718	1687	1640	1577	1492	750	156
	200	2071	2064	2043	2007	1953	1880	1781	671	163
	300	2288	2282	2261	2226	2172	2095	1989	560	169
	400	2412	2407	2389	2357	2308	2235	2130	485	173
	500	2459	2454	2437	2408	2361	2292	2189	457	175
	600	2544	2539	2524	2498	2456	2395	2301	407	179
	700	2591	2586	2572	2546	2507	2449	2361	382	181
16 km s ⁻¹	100	2257	2250	2228	2190	2131	2047	1930	1767	189
	200	2552	2547	2529	2499	2452	2383	2277	2107	182
	300	2697	2693	2680	2657	2619	2561	2470	2323	182
	400	2780	2770	2758	2737	2705	2657	2579	2445	184
	500	2892	2880	2840	2769	2738	2692	2620	2494	185
	600	3040	3033	3008	2961	2876	2756	2692	2582	186
	700	3106	3099	3078	3040	2975	2852	2729	2628	187

1.18–1.23 s. This spread is narrow compared to 16 km s⁻¹, as can be seen in Figure 2. The ZAs > 60° for 11 km s⁻¹ and ZAs > 70° for 16 km s⁻¹ are not plotted in Figure 2, as the particle does not experience temperatures that can alter the chemical composition. It is noteworthy for 11 and 16 km s⁻¹ at ZAs 70°–90° and ZAs 80°–90°, respectively, that the peak temperature is insignificant and the time spent at peak temperature is of no consequence (Table 2). The particles with higher velocities penetrate Earth’s atmosphere within smaller intervals of time, thereby generating large frictional heating, which is required to ablate their mass. The distances traveled by the particles from the beginning to the end of ablation, for entry velocities of 11 and 16 km s⁻¹, are more or less similar for various ZAs, except at 11 km s⁻¹, particle ablation starts slightly later compared to that at 16 km s⁻¹ (Figure 1). Also, the particle entering at ZA 0° penetrates slightly deeper into the Earth’s atmosphere than compared to those with higher ZAs (Figure 1). The first narrow peak corresponds to the ablation of the volatile elements (such as Na and K), which starts at an altitude of ~90 km, where their vaporization is complete (Figure 1). Further penetration of particles deeper into the atmosphere raises the temperature due to friction, where major and less volatile elements such as Fe, Mg, Si experience ablation, which is reflected in the second broader peak of Figure 1. For refractory elements such as Ca and Al, ablation depends strongly on having a larger size, higher entry velocity, and smaller ZA (Vondrak et al. 2008). The ablation percentage versus the altitude at every step of 100 m demonstrates that the ablation percentage is very small for 11 km s⁻¹ compared to 16 km s⁻¹. For a 200 μm particle size and lower ZA, the ablation percentage at every 100 m is ~10 times more for 16 km s⁻¹ than compared to 11 km s⁻¹. Similarly, for 300 μm it is ~7 times and for 400 μm it is ~3 times (Figure 1). This suggests that for different entry velocities, 11 and 16 km s⁻¹, there is a difference in the ablation percentage for smaller sizes, but the differences decrease for larger particles. Furthermore, the curve of ZA 0° is broader than that of higher ZAs for any velocity. At an entry velocity of 16 km s⁻¹ the ablation curve starts from higher altitudes compared to 11 km s⁻¹, due to the generation of heat during the interaction with air molecules at higher altitudes. This is true for all sizes and different entry velocities. The larger instantaneous ablation will change the original chemical composition, and the ablated material will eventually end up as nanometer-sized smoke in the troposphere

(Hunten et al. 1980). Previous detailed ablation studies (e.g., Flynn 1989a, 1989b; Love & Brownlee 1991) suggest better preservation of smaller particles. This can be seen in Figures 3–4 for entry velocities of 11 and 16 km s⁻¹ for various sizes 100–600 μm . The large ZAs 70°–90° and ZAs 80°–90° have a smaller effect on different sizes for 11 and 16 km s⁻¹, respectively, as the ablation is insignificant (Figures 3–4). It should be noted that a particle entering at ZA 90° with an Earth escape velocity or higher is physically impractical, as it will not descend to enter the atmosphere (Love & Brownlee 1991). A particle in horizontal flight never changes its height or ablates, as the atmospheric pressure is not high enough at that altitude, thus the particles subsequently escapes back to space (Love & Brownlee 1991). However, the increase in size and the decrease in ZA result in an increase in ablation and the change in size is relatively large if the entry velocity is amplified from 11 to 16 km s⁻¹ (Figures 3–4). Compared to a particle entering at 11 km s⁻¹, particle entering at 16 km s⁻¹ has less time to be at a peak temperature where it can deposit a large amount of heat and fuel large-scale vaporization.

Particles with an entry velocity of 11 km s⁻¹ will continue to ablate until the velocity drops to ~7 km s⁻¹; thereafter particles will be brought to thermal equilibrium slowly, alongside the temperature of the surrounding atmosphere. Likewise, for 16 km s⁻¹ the ablation will continue until ~7 km s⁻¹, but maximum ablation takes places until the particle reaches ~10 km s⁻¹ (Figure 5). The large ablation seen in particles with entry velocities of 16 km s⁻¹ and sizes >200 μm indicates a loss of those particles’ identities before they reach Earth. However, for 11 km s⁻¹ particles >400 μm can survive without large ablation (Figure 5). Based on this, if we assume that the incoming particles are uniformly distributed, then the region from ZAs 30°–90° can facilitate survival on Earth’s surface for particles with an entry velocity of 11 km s⁻¹. If particles are distributed uniformly around the Earth’s sphere then this contribution is ~2/3 (~66%) of the volume where particles (both melted and unmelted) reach the surface. Analyses of hyper-velocity impact craters found on the space-facing end of the *Long Duration Exposure Facility* spacecraft estimate micrometeorite fluxes of ~30,000 tons per annum (Love & Brownlee 1993). The region (ZAs 30°–90°) with particle survivability suggests that ~20,000 tons per annum make it to the Earth’s surface, provided all particles are entering at a low entry velocity. Considering that both melted and unmelted

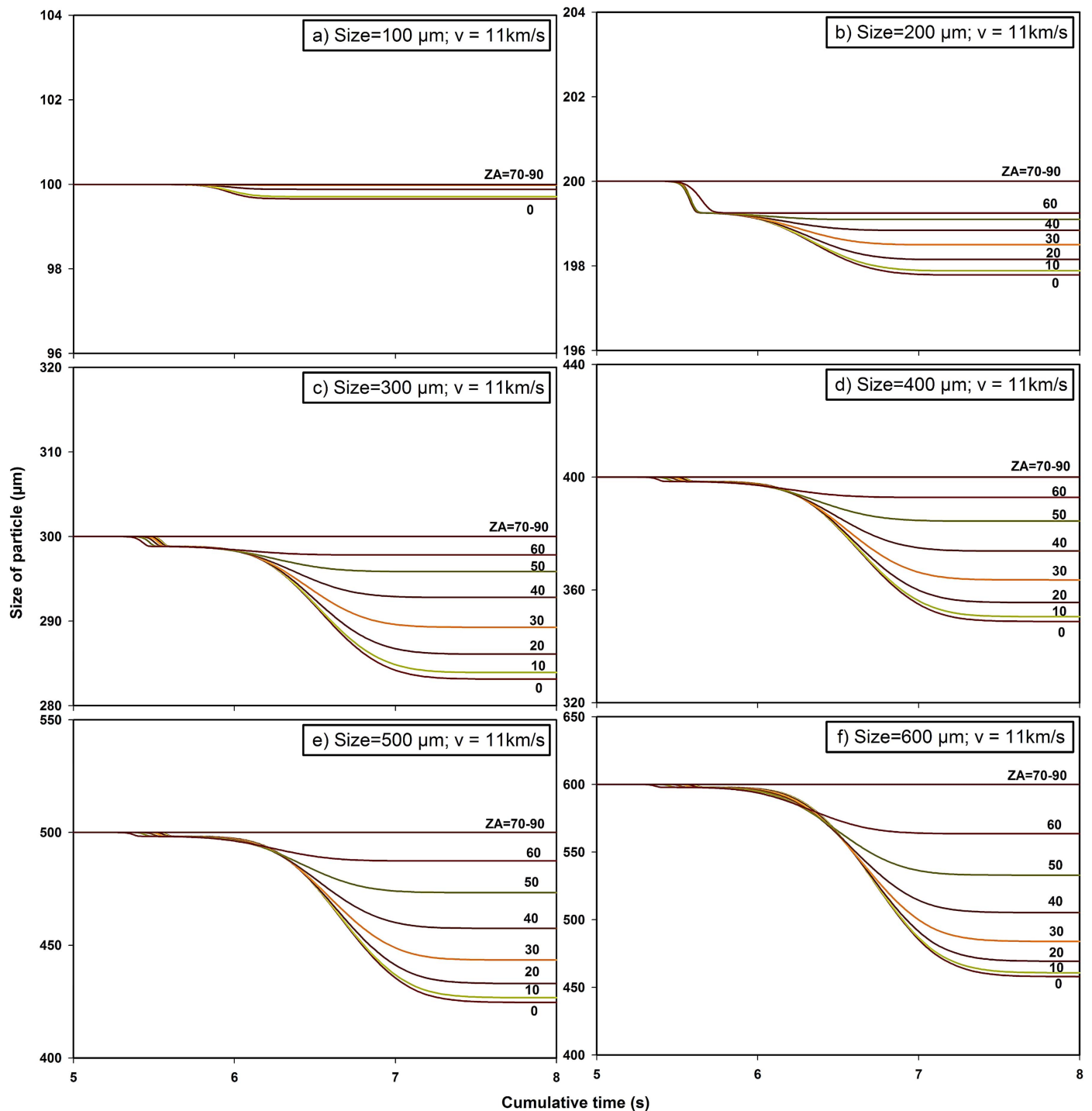


Figure 3. 11 km s^{-1} : the change in size (or diameter) of the particle for different sizes (μm) vs. the cumulative time (s) spent by it to enter the Earth's atmosphere. The number on the line in the graph is the ZA.

particles contributes 50% each to the flux based on studies done on Greenland's ice cap, the Yamato mountains, and the South Pole water well in Antarctica (Maurette et al. 1987; Yada et al. 2004; Taylor et al. 2007), the melted micrometeorites are understood to enter at ZAs 30° – 60° and particles entering with lower ZAs than indicated above will have minor contributions. The unmelted particles should make it through ZAs 60° – 90° . Meteoroids and sporadic meteors' velocity distributions relative to Earth are peaked at 16 km s^{-1} (Erickson 1968; Kessler 1969; Love & Brownlee 1993). However, there will be some contribution from particles with slightly higher velocities,

but that contribution will limit the range of ZA in which a particle can survive, as the ablation of a high-velocity particle will be close to 100%, indicating no residue will be left to reach the surface of Earth (Rudraswami et al. 2015a). The accretion rate based on hand-picking micrometeorites from Antarctica, combined with noble gas analyses from residue, agrees well with the above value (Yada et al. 2004). However, for particles in the size range of $>50 \mu\text{m}$ to a few mm, the flux may be ~ 3000 tons per annum (Taylor et al. 1998). Cziczko et al. (2001), using stratospheric aerosol chemistry, indicated that ablated sub-micron sized meteoritic residues will add

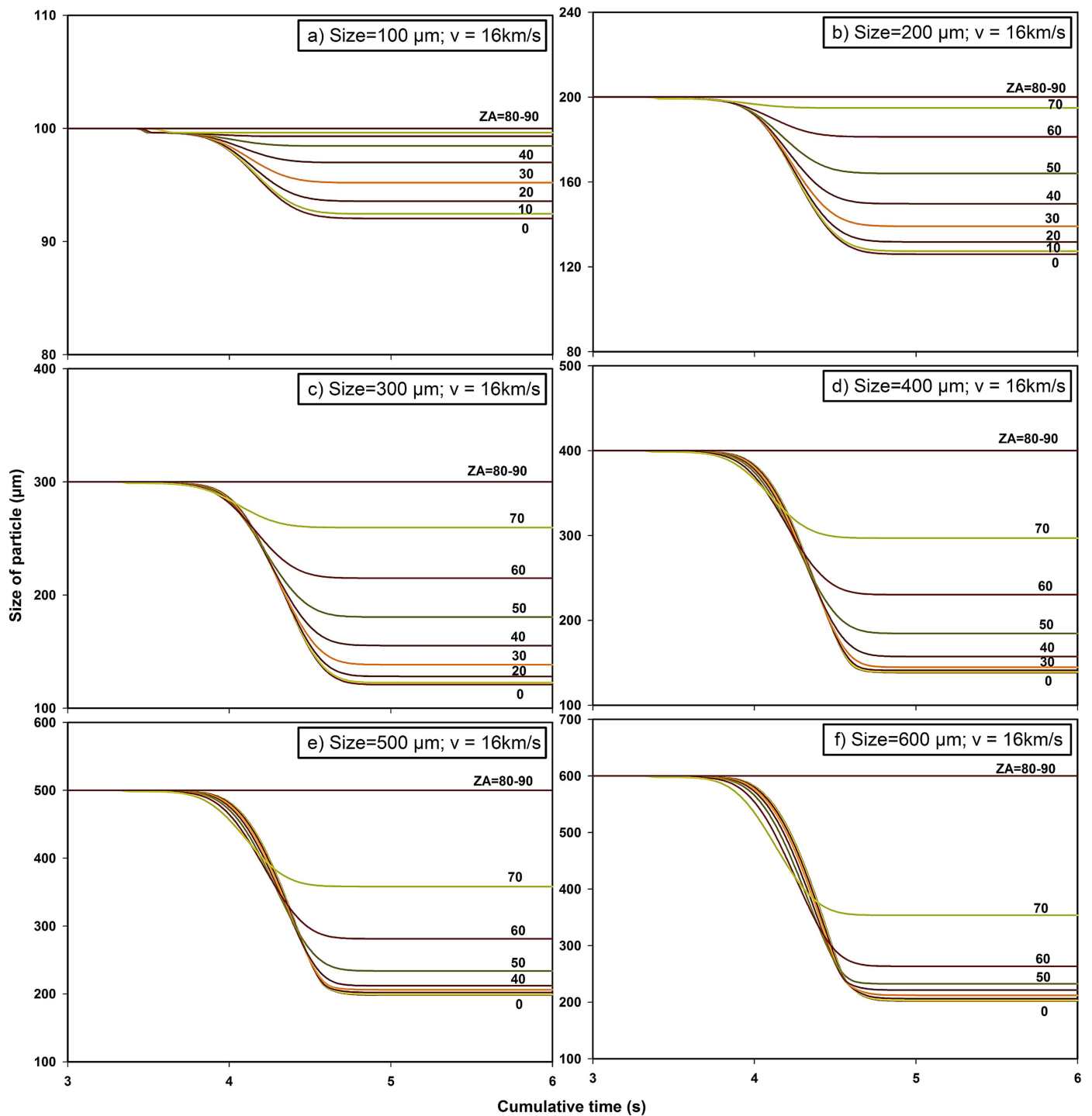


Figure 4. 16 km s^{-1} : the change in size (or diameter) of the particle for different sizes (μm) vs. the cumulative time (s) spent by it to enter the Earth's atmosphere. The number on the line in the graph is the ZA.

$\sim 4000\text{--}19000$ tons per annum (Yada et al. 2004). This evaporated material, along with estimates of handpicked extra-terrestrial particles, agrees with the flux provided by Love & Brownlee (1993).

4. VARIATION IN CHEMICAL COMPOSITIONS

The ablation due to the evaporating mass from the incoming particle results in chemical fractionation that will have quite different initial composition from that of precursor due to its

interaction with the atmosphere. The changes in chemical composition depend on the volatility of the elements and are largely disproportionate. Fe, due to its high volatility, undergoes larger ablation than Si, which is slightly more volatile than Mg (Hashimoto 1983). The different elemental compositions (oxide wt%) of dust particles with bulk CI composition show variation for different entry velocities with different sizes and a range of ZAs (Figures 6–7). The SiO_2 and FeO variation changes the stoichiometry of particles, largely depending on various entry parameters, which are discussed below.

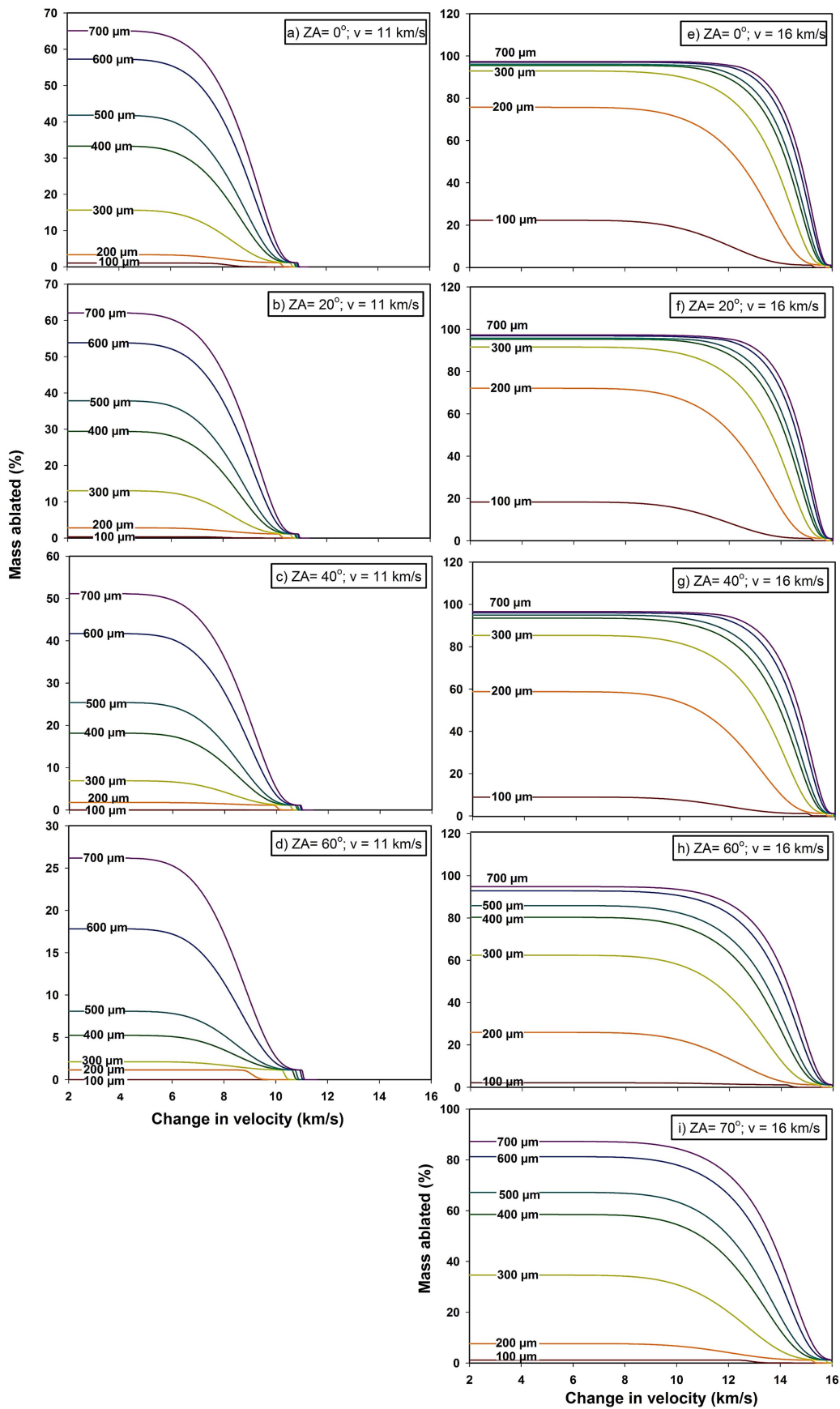


Figure 5. The change in velocity of the particle as it enters the Earth’s atmosphere with respect to the percentage of mass ablated for various sizes marked on the line for different ZAs and entry velocities. The ZA 70° for 11 km s^{-1} is not plotted, as there is no ablation, while for 16 km s^{-1} the ablation starts to drop.

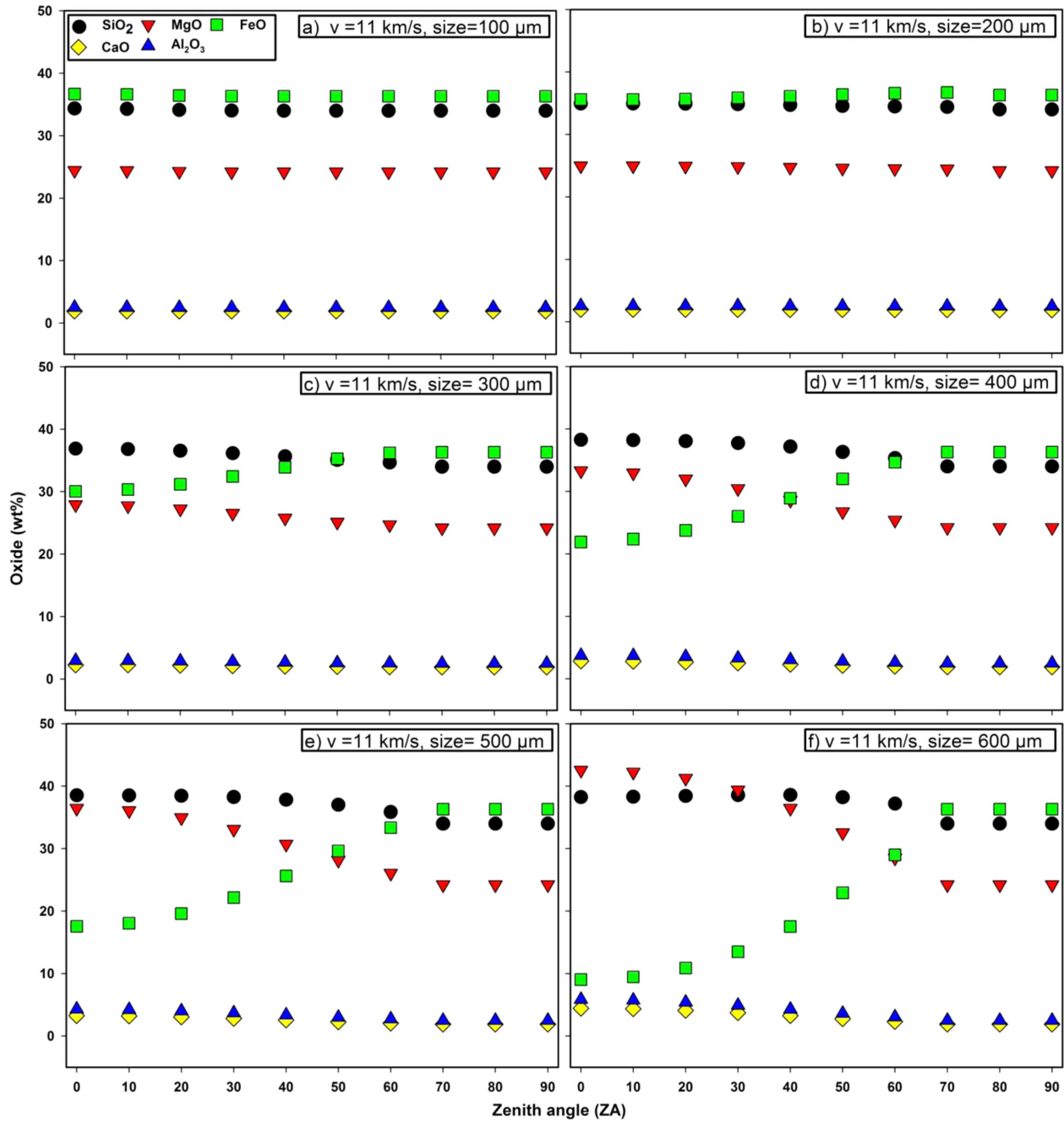


Figure 6. 11 km s^{-1} : change in oxide composition (wt%) of MgO, SiO₂, FeO, Al₂O₃, and CaO for various sizes vs. the ZA. The composition at ZA 90° is the initial composition of the particle, which is the CI composition.

The entry velocity of 11 km s^{-1} shows small variation in all major elements for particle sizes of $\sim 100 \mu\text{m}$ irrespective of any ZA. However, for particle sizes $\sim 200 \mu\text{m}$, FeO starts to deviate slightly by a few percent at lower ZAs below 30° , due to vaporization during the atmospheric entry, as can be seen in Figure 6. Nevertheless, the normalized values of Mg/Si and Fe/Si are close to CI values (Figure 8, Table 3). Beyond this size, the variation for all major elements (Mg, Si, Fe) deviates but is dominated by FeO. The enrichment of MgO and SiO₂ is compensated by the depletion of FeO. The peak temperature attained by the particle, resulting in mass-loss, plays a vital role in determining these elemental losses for various sizes and ZAs (Figure 9 and Table 2). Higher temperatures decrease the quantity of FeO due to vaporization (Hashimoto 1983). The

FeO does not extinguish at 11 km s^{-1} but is substantially depleted for large particles beyond $300 \mu\text{m}$. The change is not significantly reflected in the elemental ratio (Table 3). The interpretation based on the model result is consistent with experimental work done by Hashimoto (1983). The more refractory elements Ca and Al do not alter significantly for any size and any ZA at the entry velocity 11 km s^{-1} . Large volatility is clear from the Fe/Si ratio, where Fe/Si drops toward zero steadily for larger particle sizes at 11 and for 16 km s^{-1} the drop is rapid (Figure 8). The change in composition begins with an entry velocity of 16 km s^{-1} and vaporization of volatile element FeO. Once the FeO diminution reaches beyond 50%, the reversal of volatility takes place between SiO₂ and MgO, where MgO become more volatile

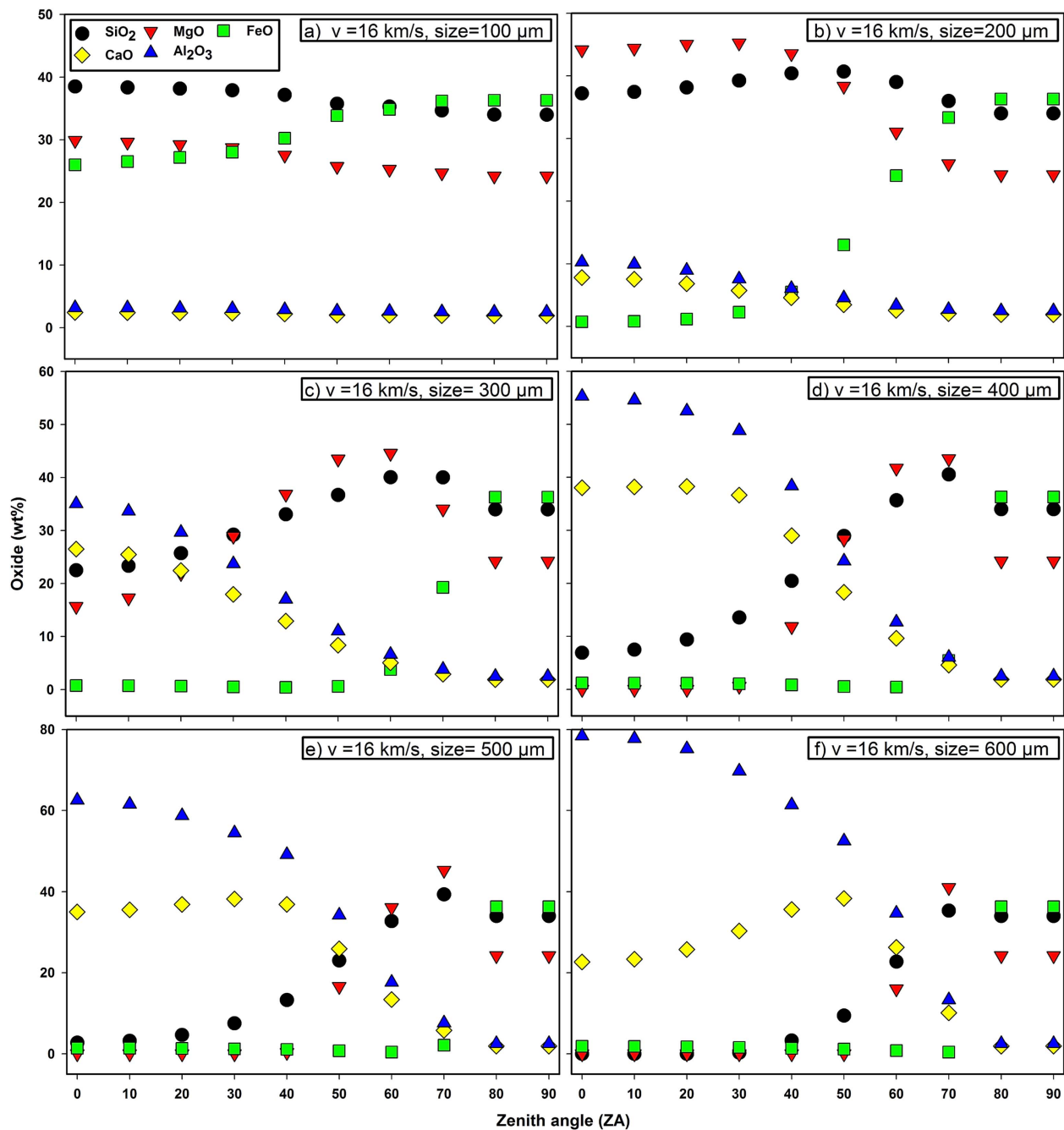


Figure 7. 16 km s^{-1} : change in oxide composition (wt%) of MgO, SiO₂, FeO, Al₂O₃, and CaO for various sizes vs. the ZA. The composition at ZA 90° is the initial composition of the particle, which is the CI composition.

than SiO₂, as can be seen in Figure 7 (Hashimoto 1983). The Mg/Si for 16 km s^{-1} raises rapidly and reaches close to ~ 1.6 (normalized to CI), then thereafter drops for all ZAs at larger sizes, due to large Mg ablation in the melt, followed by that of Si (Figure 8, Table 3). ZAs 0°–30° for Mg/Si peak at 200 μm and then drop sharply close to zero. This is due to initial Si loss that is dominant over the Mg, and subsequently Mg loss predominates. Nevertheless, the larger ZA has an elemental ratio value peak shift to larger sizes and the fall is also not as sharp as what we see at lower ZAs. This is not the case with Fe/Si, where the ratio keeps on falling, except at larger sizes beyond 400 μm and lower ZAs, there are fluctuations where most of the material is ablated. Ca/Si and Al/Si are continuously increasing due to large ablation of Si, leading to

enrichment of Ca and Al (Table 3). The theoretical prediction for 16 km s^{-1} beyond 400 μm and at lower ZA 0°–30° is that the particle is left with only Ca and Al, due to the ablation of all major elements suspended in the atmospheric cloud (Figure 7). Ca and Al have long been recognized as refractory elements, which, under favorable conditions, undergo phase changes to become hibonite or corundum, depending on the concentration of the elements present after progressive loss of the major elements.

5. CONCLUSIONS

The chemical evolution of micrometeorite particles as they enter Earth's atmosphere plays a vital role in delineating which

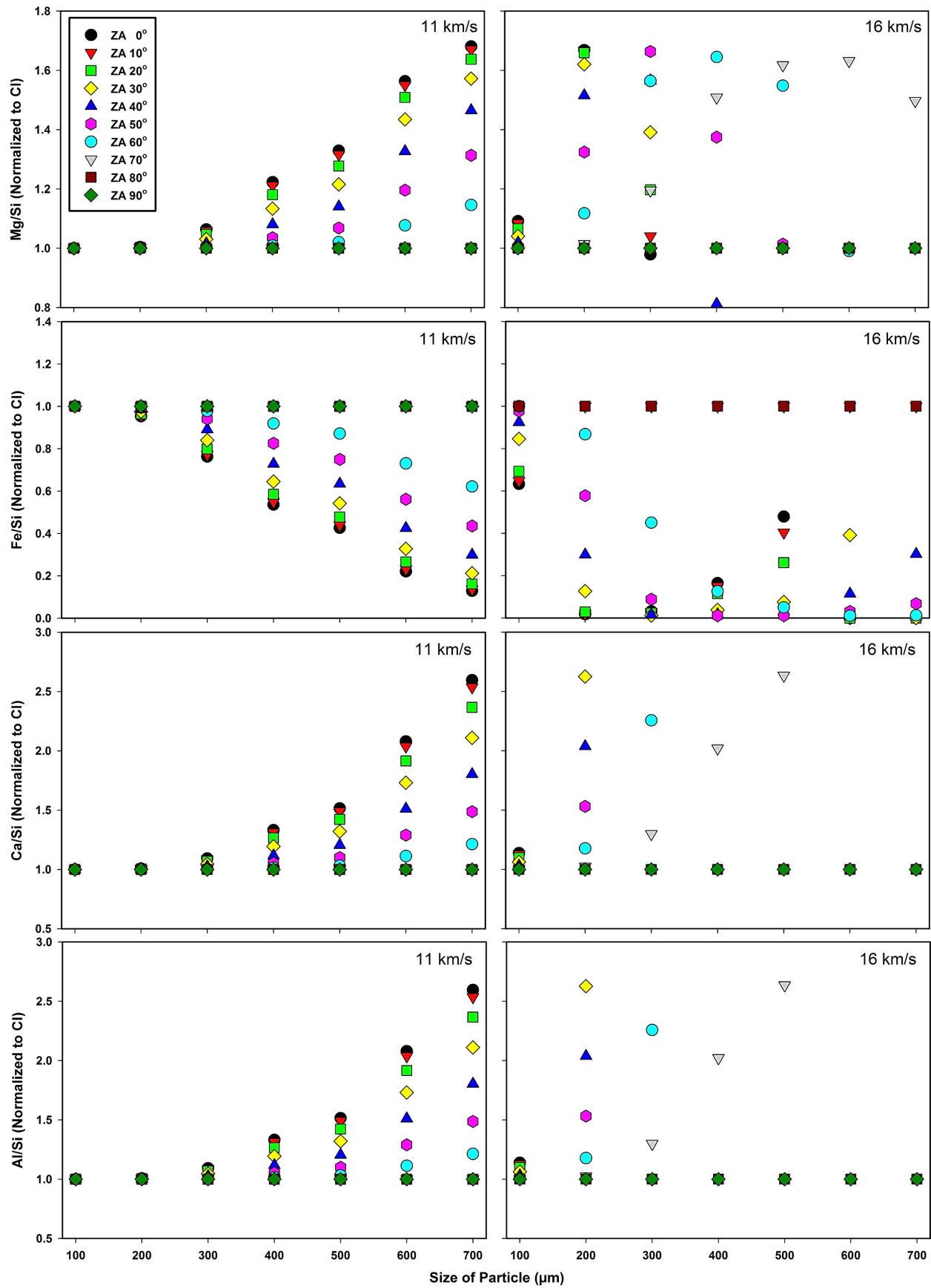


Figure 8. The elemental Mg/Si, Fe/Si, Ca/Si, and Al/Si (normalized to Cl) for different sizes and ZAs. The number on the line in the graph is the ZA.

Table 3
The Elemental Ratios Normalized to CI for Various Sizes, ZAs, and Entry Velocities

Entry Velocity	Size (μm)	ZA = 0°	10°	20°	30°	40°	50°	60°	70°	80°	90°
(a) Final Mg/Si Values (Normalized to CI)											
11 km s ⁻¹	100	1.0	1.0	1.0	1.0	1.0	1.0	1.0	1.0	1.0	1.0
	200	1.0	1.0	1.0	1.0	1.0	1.0	1.0	1.0	1.0	1.0
	300	1.1	1.1	1.0	1.0	1.0	1.0	1.0	1.0	1.0	1.0
	400	1.2	1.2	1.2	1.1	1.1	1.0	1.0	1.0	1.0	1.0
	500	1.3	1.3	1.3	1.2	1.1	1.1	1.0	1.0	1.0	1.0
	600	1.6	1.6	1.5	1.4	1.3	1.2	1.1	1.0	1.0	1.0
	700	1.7	1.7	1.6	1.6	1.5	1.3	1.1	1.0	1.0	1.0
16 km s ⁻¹	100	1.1	1.1	1.1	1.0	1.0	1.0	1.0	1.0	1.0	1.0
	200	1.7	1.7	1.7	1.6	1.5	1.3	1.1	1.0	1.0	1.0
	300	1.0	1.0	1.2	1.4	1.6	1.7	1.6	1.2	1.0	1.0
	400	0.1	0.8	1.4	1.6	1.5	1.0	1.0
	500	0.0	1.0	1.5	1.6	1.0	1.0
	600	1.0	1.6	1.0	1.0
	700	0.1	1.5	1.0	1.0
(b) Final Fe/Si values (Normalized to CI)											
11 km s ⁻¹	100	1.0	1.0	1.0	1.0	1.0	1.0	1.0	1.0	1.0	1.0
	200	1.0	1.0	1.0	1.0	1.0	1.0	1.0	1.0	1.0	1.0
	300	0.8	0.8	0.8	0.8	0.9	0.9	1.0	1.0	1.0	1.0
	400	0.5	0.5	0.6	0.6	0.7	0.8	0.9	1.0	1.0	1.0
	500	0.4	0.4	0.5	0.5	0.6	0.7	0.9	1.0	1.0	1.0
	600	0.2	0.2	0.3	0.3	0.4	0.6	0.7	1.0	1.0	1.0
	700	0.1	0.1	0.2	0.2	0.3	0.4	0.6	1.0	1.0	1.0
16 km s ⁻¹	100	0.6	0.6	0.7	0.8	0.8	0.9	1.0	1.0	1.0	1.0
	200	0.0	0.0	0.0	0.1	0.1	0.3	0.6	0.9	1.0	1.0
	300	0.0	0.0	0.0	0.0	0.0	0.0	0.1	0.5	1.0	1.0
	400	0.2	0.2	0.1	0.1	0.0	0.0	0.0	0.1	1.0	1.0
	500	0.5	0.4	0.3	0.1	0.1	0.0	0.0	0.1	1.0	1.0
	600	5.6	0.4	0.1	0.0	0.0	1.0	1.0
	700	0.3	0.1	0.0	1.0	1.0
(c) Final Ca/Si values (Normalized to CI)											
11 km s ⁻¹	100	1.0	1.0	1.0	1.0	1.0	1.0	1.0	1.0	1.0	1.0
	200	1.0	1.0	1.0	1.0	1.0	1.0	1.0	1.0	1.0	1.0
	300	1.1	1.1	1.1	1.0	1.0	1.0	1.0	1.0	1.0	1.0
	400	1.3	1.3	1.3	1.2	1.1	1.1	1.0	1.0	1.0	1.0
	500	1.5	1.5	1.4	1.3	1.2	1.1	1.0	1.0	1.0	1.0
	600	2.1	2.0	1.9	1.7	1.5	1.3	1.1	1.0	1.0	1.0
	700	2.6	2.5	2.4	2.1	1.8	1.5	1.2	1.0	1.0	1.0
16 km s ⁻¹	100	1.1	1.1	1.1	1.1	1.0	1.0	1.0	1.0	1.0	1.0
	200	3.8	3.6	3.2	2.6	2.0	1.5	1.2	1.0	1.0	1.0
	300	21	20	16	11	7.0	4.1	2.3	1.3	1.0	1.0
	400	99	92	73	48	25	11	4.8	2.0	1.0	1.0
	500	231	201	142	91	50	20	7.3	2.6	1.0	1.0
	600	196	73	21	5.1	1.0	1.0
	700	160	45	8.4	1.0	1.0
(d) Final Al/Si values (Normalized to CI)											
11 km s ⁻¹	100	1.0	1.0	1.0	1.0	1.0	1.0	1.0	1.0	1.0	1.0
	200	1.0	1.0	1.0	1.0	1.0	1.0	1.0	1.0	1.0	1.0
	300	1.1	1.1	1.1	1.0	1.0	1.0	1.0	1.0	1.0	1.0
	400	1.3	1.3	1.3	1.2	1.1	1.1	1.0	1.0	1.0	1.0
	500	1.5	1.5	1.4	1.3	1.2	1.1	1.0	1.0	1.0	1.0
	600	2.1	2.0	1.9	1.7	1.5	1.3	1.1	1.0	1.0	1.0
	700	2.6	2.5	2.4	2.1	1.8	1.5	1.2	1.0	1.0	1.0
16 km s ⁻¹	100	1.1	1.1	1.1	1.1	1.0	1.0	1.0	1.0	1.0	1.0
	200	3.8	3.6	3.2	2.6	2.0	1.5	1.2	1.0	1.0	1.0
	300	21	20	16	11	7.0	4.1	2.3	1.3	1.0	1.0
	400	109	99	76	49	26	11	4.8	2.0	1.0	1.0

Table 3
(Continued)

Entry Velocity	Size (μm)	ZA = 0°	10°	20°	30°	40°	50°	60°	70°	80°	90°
	500	314	265	172	99	50	20	7.3	2.6	1.0	1.0
	600	257	76	21	5.1	1.0	1.0
	700	199	45	8.4	1.0	1.0

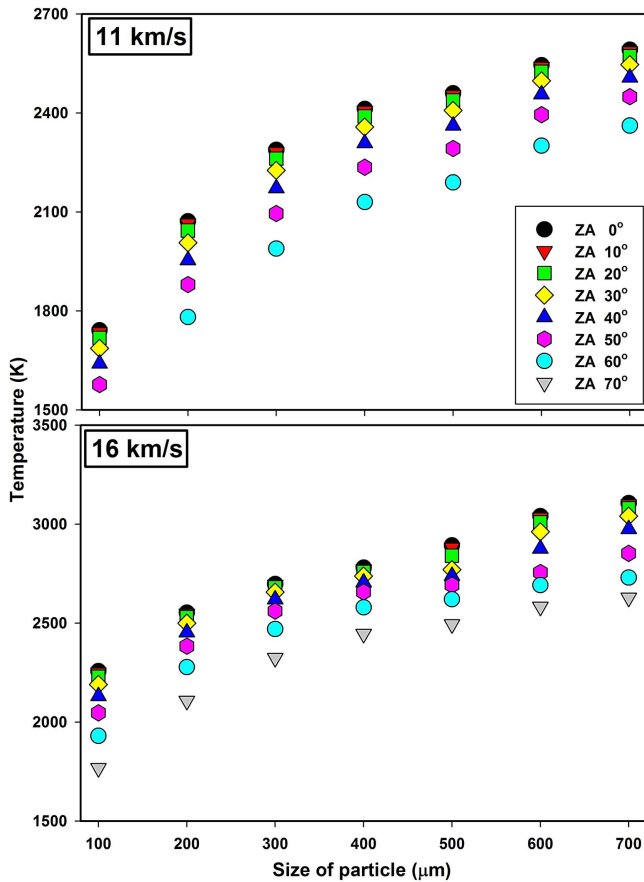


Figure 9. Distribution of temperature for various sizes (100–700 μm) at various ZAs for entry velocities 11 and 16 km s^{-1} . The temperature (K) experienced by particles entering at ZAs $\geq 70^\circ$ with entry velocity 11 km s^{-1} is below 750 K, and hence is not visible in range plotted.

processes and which stages of deviation are relevant for attaining these particles' precursor compositions. The information provided by this study provides an understanding of the stoichiometry, chemical alteration from the initial composition, ablation, and mass-loss during atmospheric entry for different entry parameters such as size, entry velocity, and zenith angle. Here we have demonstrated that for an entry velocity of 11 km s^{-1} , the major element chemical compositions are preserved for particle sizes $<400 \mu\text{m}$, beyond which FeO largely ablates. The ablation is drastic for particles with an entry velocity of 16 km s^{-1} , where particle elemental ratios vary largely and major elements get depleted, leaving behind refractory elements Al and Ca. The model indicates that for an entry velocity of 11 km s^{-1} , ZAs 30° – 60° contribute to melted particles, while ZAs 70° – 90° are dominated by unmelted particles. For particles with a velocity of 16 km s^{-1} , the contribution of melted particles gets restricted to narrow ZAs due to large-scale ablation, and that for unmelted particles is restricted to ZAs $>80^\circ$. Overall, the survivability of the

particles at low entry velocities with ZAs 30° – 90° seems feasible and is estimated to be $\sim 20,000$ tons/annum.

This research was supported by the GEOSINKS, MOES-PMN, and the PLANEX projects. The CABMOD model development is supported by the European Research Council (project 291332—CODITA). This is NIO's contribution No. 5958.

REFERENCES

- Bohren, C. F., & Huffman, D. R. 1983, *Absorption and Scattering of Light by Small Particles* (New York: Wiley-Interscience)
- Brownlee, D., Tsou, P., Aléon, J., et al. 2006, *Sci*, **314**, 1711
- Brownlee, D. E. 2001, in *Accretion of Extraterrestrial Matter Throughout Earth's History*, ed. B. Peucker-Ehrenbrink & B. Schmitz (New York: Kluwer/Plenum)
- Brownlee, D. E. 2014, *AREPS*, **42**, 179
- Brownlee, D. E., Bates, B., & Schramm, L. 1997, *M&PS*, **32**, 157
- Carrillo-Sánchez, J. D., Plane, J. M. C., Feng, W., Nesvorný, D., & Janches, D. 2015, *GeoRL*, **42**, 6518
- Cziczo, D. J., Thomson, D. S., & Murphy, D. M. 2001, *Sci*, **291**, 1772
- Dermott, S. F., Jayaraman, S., Xu, Y. L., Gustafson, B. A. S., & Liou, J. C. 1994, *Natur*, **369**, 719
- Erickson, J. E. 1968, *JGR*, **73**, 3721
- Flynn, G. J. 1989a, *LPSC*, **19**, 673
- Flynn, G. J. 1989b, *Icar*, **77**, 287
- Hashimoto, A. 1983, *GeocJ*, **17**, 111
- Hunten, D. M., Turco, R. P., & Toon, O. B. 1980, *JAtS*, **37**, 1342
- Kessler, D. J. 1969, *AIAAJ*, **7**, 2337
- Kortenkamp, S. J., Dermott, S. F., Fogle, D., & Grogan, K. 2001, in *Accretion of Extraterrestrial Matter Throughout Earth's History*, ed. B. Peucker-Ehrenbrink & B. Schmitz (New York: Kluwer/Plenum)
- Krot, A. N., Keil, K., Goodrich, C. A., Scott, E. R. D., & Weisberg, M. K. 2003, in *Classification of Meteorites. In Meteorites, Comets, and Planets. In Treatise on Geochemistry*, Vol. 1, ed. A. M. Davis (Amsterdam: Elsevier)
- Kurat, G., Koeberl, C., Presper, T., Brandstätter, F., & Maurette, M. 1994, *GeCoA*, **58**, 3879
- Lal, D., & Jull, A. T. J. 2002, *APJ*, **576**, 1090
- Lodders, K., & Fegley, B., Jr. 1998, *The Planetary Scientist's Companion* (New York: Oxford Univ. Press)
- Love, S. G., & Brownlee, D. E. 1991, *Icar*, **89**, 26
- Love, S. G., & Brownlee, D. E. 1993, *Sci*, **262**, 550
- Love, S. G., Joswiak, D. J., & Brownlee, D. E. 1994, *Icar*, **111**, 227
- Mason, B. 1971, *Handbook of Elemental Abundances of the Elements in Meteorites* (Newark: Gordon and Breach)
- Maurette, M., Jéhanno, C., Robin, E., & Hammer, C. 1987, *Natur*, **328**, 699
- Nesvorný, D., Janches, D., Vokrouhlický, D., et al. 2011, *ApJ*, **743**, 129
- Nesvorný, D., Jenniskens, P., Levison, H. F., et al. 2010, *ApJ*, **713**, 816
- Peucker-Ehrenbrink, B., & Ravizza, G. 2000, *GeCoA*, **64**, 1965
- Plane, J. M. C. 2012, *Chem. Soc. Rev.*, **41**, 6507
- Prasad, M. S., Rudraswami, N. G., & Panda, D. K. 2013, *JGR*, **118**, 2381
- Rudraswami, N. G., Prasad, M. S., Babu, E. V. S. S. K., et al. 2012, *GeCoA*, **99**, 110
- Rudraswami, N. G., Prasad, M. S., Dey, S., et al. 2015a, *APJ*, **814**, 78
- Rudraswami, N. G., Prasad, M. S., Plane, J. M. C., et al. 2014, *GeCoA*, **131**, 247
- Rudraswami, N. G., Shyam Prasad, M., Dey, S., et al. 2016a, *APJ*, **831**, 197
- Rudraswami, N. G., Shyam Prasad, M., Jones, R. H., & Nagashima, K. 2016b, *GeCoA*, **194**, 1
- Rudraswami, N. G., Shyam Prasad, M., Nagashima, K., & Jones, R. H. 2015b, *GeCoA*, **164**, 53
- Rudraswami, N. G., Ushikubo, T., Nakashima, D., & Kita, N. T. 2011, *GeCoA*, **75**, 7596
- Schaefer, L., & Fegley, B. 2005, *EMP*, **95**, 413

- Sears, D. W., & Dodd, R. T. 1988, in *Meteorites and the Early Solar System*, ed. J. F. Kerridge & M. S. Matthews (Tucson, AZ: Univ. Arizona Press)
- Taylor, S., Herzog, G. F., & Delaney, J. S. 2007, *M&PS*, **42**, 223
- Taylor, S., Lever, J. H., & Harvey, R. P. 1998, *Natur*, **392**, 899
- Taylor, S., Lever, J. H., & Harvey, R. P. 2000, *M&PS*, **35**, 651
- Taylor, S., Matrajt, G., & Guan, Y. 2012, *M&PS*, **47**, 550
- Vondrak, T., Plane, J. M. C., Broadley, S., & Janches, D. 2008, *ACP*, **8**, 7015
- Yada, T., Nakamura, T., Noguchi, T., et al. 2005, *GeCoA*, **69**, 5789
- Yada, T., Nakamura, T., Takaoka, N., et al. 2004, *EPS*, **56**, 67